Research Square

Preprints are preliminary reports that have not undergone peer review.
They should not be considered conclusive, used to inform clinical practice,
or referenced by the media as validated information.

Functional Connectivity Gradients Reveal Cortical Hierarchical Reorganization Across the Cirrhosis–Hepatic Encephalopathy Spectrum

Minghui Mao
Fuzong Teaching Hospital of Fujian University of Traditional Chinese Medicine (900th Hospital)
Guoqiang Wei
Fujian University of Traditional Chinese Medicine
Xiaoyang Wang
Fuzong Teaching Hospital of Fujian University of Traditional Chinese Medicine (900th Hospital)
Shuoxuan Huang
Capital Medical University
Chengkun Hong
Fuzong Teaching Hospital of Fujian University of Traditional Chinese Medicine (900th Hospital)
Li Chen
Fuzong Clinical Medical College of Fujian Medical University
Hao Huang
Fuzong Teaching Hospital of Fujian University of Traditional Chinese Medicine (900th Hospital)
A ling Shen
Fujian University of Traditional Chinese Medicine
Liyuan Fu
fu3138706250126.com

Fuzong Teaching Hospital of Fujian University of Traditional Chinese Medicine (900th Hospital)

Research Article

Keywords: ammonia, functional connectivity gradients, brain mapping, magnetic resonance imaging, psychometric hepatic encephalopathy score

Posted Date: November 1st, 2026

DOI: https://doi.org/10.21203/rs.3.rs-11271162/v1

License: This work is licensed under a Creative Commons Attribution 4.0 International License.
Read Full License

Additional Declarations: No competing interests reported.

Abstract

Background

Hepatic encephalopathy (HE) is a common neurocognitive complication of cirrhosis, but how macroscale cortical hierarchy is reorganized across the cirrhosis–HE spectrum remains incompletely understood. We characterized functional connectome gradient alterations across clinically defined cirrhosis stages and examined their clinical correlates.

Methods

This cross-sectional study included 104 participants: 35 patients with HE, 33 with cirrhosis without HE (NHE), and 36 healthy controls. Resting-state functional MRI was used to derive the first three connectivity gradients (G1–G3). Group differences were assessed at global, network, and cortical-parcel levels, and associations with blood ammonia, liver disease severity, and cognition were examined in patients with cirrhosis.

Results

Both NHE and HE showed reduced G1 range and variance versus healthy controls, indicating compression of the sensorimotor-to-transmodal hierarchy. Both groups showed higher somatomotor G1 and lower control and default mode G1, whereas HE additionally showed lower limbic G1. The only significant HE–NHE parcel-level difference involved the right temporal pole. Higher ammonia was associated with higher somatomotor G1 and lower control and default mode G1, while greater liver disease severity was associated mainly with lower limbic and default mode G1. Poorer cognition showed broadly corresponding associations. G2 and G3 did not differ among groups, and the main findings remained robust in sensitivity analyses.

Conclusion

NHE and HE showed largely shared compression of the sensorimotor-to-transmodal hierarchy, with more selective HE-associated alterations, particularly in temporolimbic regions. These abnormalities were associated with ammonia burden, liver disease severity, and cognitive impairment, supporting altered cortical functional hierarchy as a clinically relevant systems-level phenotype across the cirrhosis–HE spectrum.

Introduction

Hepatic encephalopathy (HE) is a neurocognitive syndrome arising in the setting of hepatic insufficiency or portosystemic shunting and represents a clinically important complication of cirrhosis [1–3]. Its

manifestations span impaired attention, psychomotor slowing, and executive dysfunction to behavioral abnormalities, altered consciousness, and coma [1, 4]. Covert HE, including minimal HE and West Haven grade I HE, is clinically relevant because it is associated with subsequent overt HE, hospitalization, and adverse outcomes [5]. Importantly, cognitive and brain functional abnormalities may already be present in patients with cirrhosis who do not meet diagnostic criteria for HE [6, 7]. Characterizing brain alterations across the cirrhosis–HE spectrum may therefore provide insight into the neural organization underlying cognitive dysfunction in cirrhosis.

Resting-state functional magnetic resonance imaging (rs-fMRI) has revealed widespread functional abnormalities in cirrhosis, involving sensorimotor, visual association, frontal, and posterior parietal regions [6–8]. At the network level, abnormalities have been reported in the default mode, somatomotor, and cognitive control systems [6, 7, 9], while whole-brain analyses further indicate disrupted coordination among large-scale functional networks [10]. Together, these findings suggest that cirrhosis-related brain dysfunction involves coordinated alterations across distributed functional systems rather than isolated regional abnormalities. However, conventional approaches based on regional activity, pairwise connectivity, or discrete network boundaries do not fully capture the continuous organizational architecture linking these systems.

The cerebral cortex is organized not only into discrete functional networks but also along continuous hierarchical axes extending from primary sensorimotor regions to transmodal association cortex [11, 12]. Functional connectivity gradient analysis summarizes similarities in whole-brain connectivity profiles into low-dimensional axes, providing an integrated representation of macroscale cortical organization [12–14]. The principal gradient (G1) typically extends from primary sensorimotor systems to the default mode network, whereas subsequent gradients capture additional distinctions among sensory and higher-order systems [12, 13]. This framework has revealed hierarchical reorganization across a range of neurological, psychiatric, and systemic disorders [15–19], providing a systems-level perspective that complements conventional regional and network-based analyses. Previous studies have identified reproducible abnormalities of the principal functional gradient in cirrhosis and suggested stage-related disruption of cortical hierarchy [20]. Nevertheless, how these abnormalities are organized across the broader clinically defined cirrhosis–HE spectrum, and how they relate to clinical burden and cognitive dysfunction, remains incompletely understood. We therefore compared functional connectivity gradients among healthy controls (HCs), patients with cirrhosis without HE (NHE), and patients with HE at the global, functional-network, and cortical-parcel levels, and further examined their associations with blood ammonia levels, liver disease severity, and cognitive performance. We hypothesized that cirrhosis would be associated with disruption of the principal sensorimotor-to-transmodal hierarchy, with additional alterations in HE, and that these abnormalities would be associated with greater disease burden and poorer cognitive performance.

Materials and methods

Study design and participants

The study protocol was approved by the institutional review board of the participating hospital (approval no. 2025-087) and registered with the Chinese Clinical Trial Registry (ChiCTR2500106101). Written informed consent was obtained from all participants, and the study complied with the Declaration of Helsinki.

Patients aged 18–75 years with cirrhosis were consecutively recruited from the outpatient clinic and inpatient service between January 2025 and March 2026. Cirrhosis was diagnosed according to clinical practice guidelines [21]. Two hepatologists independently assessed eligibility and assigned West Haven grades [2, 3]. HCs without liver or systemic diseases were recruited from the same hospital and frequency-matched by age, sex, and education. Exclusion criteria included alcohol-related cirrhosis or heavy alcohol consumption within the previous 6 months (> 60 g/day for men and > 40 g/day for women) [22]; psychoactive substance use disorder or related treatment within 6 months (except nicotine use); MRI contraindications; hepatic malignancy or rapidly progressive liver failure; West Haven grade 3 or 4 HE; and incomplete MRI data or rs-fMRI data failing predefined quality control. The final sample included 104 participants: 35 HE patients (57.5 ± 6.4 years; 23 men), 33 NHE patients (55.7 ± 7.2 years; 19 men), and 36 HCs (55.4 ± 7.9 years; 24 men).

Clinical and psychometric assessments were performed on the day of MRI. Patients were classified into the HE group if they had covert or overt HE at enrollment or a documented overt HE episode (West Haven grade ≥ 2) within the previous month. A documented overt HE episode was verified from hepatology records, including West Haven grading and HE-directed treatment. At enrollment, covert HE included minimal HE and West Haven grade 1 HE, whereas overt HE was defined as West Haven grade 2 HE. Minimal HE was defined as West Haven grade 0 with PHES ≤ − 4. NHE was defined as no documented history of overt HE based on medical record review and patient/caregiver interview, West Haven grade 0, and PHES > − 4 [23, 24]. Medication use before and at enrollment, including HE-directed therapy, was recorded for all patients. Lactulose use at the time of MRI was confined to the HE group and reflected secondary prophylaxis in patients with recent overt HE. PHES obtained on the MRI day was used for classification because minimal HE status may fluctuate.

Clinical and neuropsychological assessments

On the day of MRI, trained researchers administered the Mini-Mental State Examination (MMSE) and Montreal Cognitive Assessment (MoCA) [25, 26], together with the PHES [23], in a quiet, standardized setting. The PHES was calculated using Chinese norms adjusted for age and education [23]. In patients, peripheral venous blood was collected within 3 days before MRI for measurement of blood ammonia, serum sodium, and estimated glomerular filtration rate (eGFR). Liver disease severity was assessed using the Child-Pugh and Model for End-Stage Liver Disease (MELD) scores [27, 28].

MRI data acquisition and preprocessing

MRI data were acquired on a 3.0-T United Imaging uMR 770 scanner equipped with a 32-channel head coil. The protocol included high-resolution T1-weighted imaging, rs-fMRI, T2-weighted imaging, and T2-FLAIR to assess structural abnormalities. Foam padding and earplugs were used to reduce head motion and scanner noise. During rs-fMRI, participants were instructed to keep their eyes closed, remain awake and relaxed, and avoid deliberate mental activity. Detailed MRI acquisition parameters are provided in the Supplementary Methods.

The rs-fMRI data were preprocessed using the Data Processing & Analysis for Brain Imaging toolbox, which is based on Statistical Parametric Mapping [29]. Detailed preprocessing procedures are provided in the Supplementary Methods. Field-map- or reversed-phase-encoding-based susceptibility distortion correction was not performed because the required acquisitions were unavailable. Data were excluded due to poor image quality, preprocessing failure, excessive head motion, or insufficient remaining volumes after motion correction.

Functional connectivity gradient analysis

Individual functional connectivity gradients were generated using BrainSpace (Fig. 1). Based on the Schaefer 400-parcel seven-network atlas [30, 31], Pearson correlations between parcel-wise time series were calculated to generate 400 × 400 connectivity matrices, followed by Fisher r-to-z transformation. Diagonal and negative values were set to zero to obtain a non-negative connectivity representation before sparsification and diffusion embedding. For each parcel, the strongest 10% of connections were retained, and cosine similarity was used to construct the affinity matrix [12, 14]. Diffusion map embedding was applied to derive low-dimensional connectivity gradients [32]. Parameters were set as recommended ($\alpha = 0.5$, diffusion time = 0, random seed = 42), and 10 components were retained for alignment [14].

A cohort-specific HC reference was generated by averaging connectivity matrices from 36 HCs. This reference was aligned to the BrainSpace group-average Schaefer-400 template using 10-dimensional orthogonal Procrustes rotation, and individual gradients were subsequently aligned to this reference to ensure consistent component ordering and orientation across participants [14]. The first three aligned gradients (G1–G3) were analyzed, explaining 46.8% of variance.

For each gradient, parcel-wise mean, range, and variance were calculated. Network-level gradient values were obtained by averaging parcels within seven Yeo networks. Parcel-level analyses were performed to identify regional gradient alterations.

Statistical analysis

Statistical analyses were performed using R 4.4.2. Demographic, clinical, and cognitive variables were compared using one-way analysis of variance or the Kruskal–Wallis test, as appropriate, followed by pairwise comparisons when the omnibus test was significant. Gradient measures were compared using

analysis of covariance, with age, sex, and years of education included as covariates. Partial Pearson correlations were used to assess associations between gradient measures and clinical or cognitive variables in the pooled cirrhosis cohort (HE and NHE), controlling for the same covariates.

The Benjamini–Hochberg false discovery rate (FDR) procedure was used to control for multiple comparisons. For global analyses, FDR correction was performed separately within each gradient across the three global metrics (mean, range, and variance). For network-level group comparisons, FDR correction was performed separately within each gradient across the seven Yeo networks. Post hoc pairwise comparisons following significant omnibus effects were also FDR-corrected. Parcel-level group comparisons were FDR-corrected across 400 Schaefer cortical parcels within each contrast. For clinical association analyses, only G1 networks and cortical parcels showing significant between-group differences were examined. At the network level, FDR correction was applied across 32 tests (4 significant networks × 8 clinical measures). At the parcel level, FDR correction was applied across 656 tests (82 significant parcels × 8 clinical measures).

Sensitivity analyses were performed by reconstructing gradients at 5.0%, 10.0%, and 15.0% connectivity sparsity thresholds and by repeating the primary models with mean Jenkinson framewise displacement (FD) included as an additional covariate. All tests were two-sided, with statistical significance defined as $P < 0.05$ or FDR-adjusted $P < 0.05$, as appropriate.

Results

Clinical and demographic characteristics

Figure 2 illustrates the participant screening, exclusion, and final inclusion process. Table 1 summarizes the demographic, clinical, and neuropsychological characteristics of the HE, NHE, and HC groups. A total of 104 participants were included in the final analysis: 35 in the HE group, 33 in the NHE group, and 36 in the HC group. No significant differences were observed among the three groups in age, sex, years of education, or mean framewise displacement (mean FD). Compared with the HC group, both the HE and NHE groups had lower MoCA, MMSE, and PHES scores (all $P < 0.001$). In addition, the HE group had lower PHES scores and higher Child–Pugh scores and blood ammonia levels than the NHE group (all $P < 0.001$). MELD scores, serum sodium levels, and eGFR did not differ significantly between the HE and NHE groups.

Table 1
Demographic, Clinical, and Neuropsychological Characteristics of Participants in the HE, NHE, and HC Groups

Characteristic	HE group (n = 35)	NHE group (n = 33)	HC group (n = 36)	P
Age (y)[a]	57.49 ± 6.42	55.67 ± 7.24	55.42 ± 7.88	0.427
Sex, n (%)				0.695
Male	23 (65.7)	19 (57.6)	24 (66.7)	
Female	12 (34.3)	14 (42.4)	12 (33.3)	
Education (y)[a]	7.79 ± 2.16	8.05 ± 3.00	7.94 ± 2.39	0.913
Etiology, n (%)				0.886
Viral hepatitis	27 (77.1)	26 (78.8)	NA	
Autoimmune	7 (20.0)	7 (21.2)	NA	
Mixed (viral hepatitis + autoimmune)	1 (2.9)	0 (0.0)	NA	
Lactulose use at MRI, n (%)	5 (14.3)	0 (0.0)	NA	0.054
Mean FD[a](mm)	0.11 ± 0.05	0.12 ± 0.05	0.12 ± 0.04	0.312
MoCA[b]	26.00 (25.00, 27.50)	28.00 (27.00, 29.00)	30.00 (29.00, 30.00)	< 0.001[c]
MMSE[b]	27.00 (26.00, 28.00)	29.00 (28.00, 30.00)	30.00 (29.75, 30.00)	< 0.001[c]
PHES[b]	-5.00 (-7.00, -4.00)	-1.00 (-2.00, 0.00)	0.00 (0.00, 0.00)	< 0.001[c]
MELD score[a]	12.74 ± 4.66	10.82 ± 3.80	NA	0.068
Child-Pugh[b]	8.00 (7.00, 10.00)	6.00 (5.00, 7.00)	NA	< 0.001

[a] Data are presented as mean ± SD.

[b] Data are presented as median (IQR).

[c] Pairwise comparisons showed significant differences between HE and NHE, between HE and HC, and between NHE and HC groups; Mann–Whitney U tests with Holm correction.

Abbreviations: HE, hepatic encephalopathy; NHE, cirrhosis without hepatic encephalopathy; HC, healthy control; MMSE, Mini-Mental State Examination; MoCA, Montreal Cognitive Assessment; PHES, Psychometric Hepatic Encephalopathy Score; MELD, Model for End-Stage Liver Disease; eGFR, estimated glomerular filtration rate; FD, framewise displacement.

Characteristic	HE group (n = 35)	NHE group (n = 33)	HC group (n = 36)	P
Ammonia (μmol/L)[b]	92.40 (60.75, 123.35)	35.30 (26.60, 68.80)	NA	< 0.001
Sodium[a]	140.11 ± 3.35	141.45 ± 2.90	NA	0.082
eGFR[b]	98.83 (82.34, 110.62)	104.23 (85.22, 113.75)	NA	0.191
[a] Data are presented as mean ± SD.				
[b] Data are presented as median (IQR).				
[c] Pairwise comparisons showed significant differences between HE and NHE, between HE and HC, and between NHE and HC groups; Mann–Whitney U tests with Holm correction.				
Abbreviations: HE, hepatic encephalopathy; NHE, cirrhosis without hepatic encephalopathy; HC, healthy control; MMSE, Mini-Mental State Examination; MoCA, Montreal Cognitive Assessment; PHES, Psychometric Hepatic Encephalopathy Score; MELD, Model for End-Stage Liver Disease; eGFR, estimated glomerular filtration rate; FD, framewise displacement.				

Functional connectivity gradient alterations

G1-G3 together explained 46.8% of the variance in connectome organization, with G1, G2, and G3 accounting for 24.6%, 13.6%, and 8.6%, respectively. G1 extended from the primary visual and somatomotor networks to the transmodal DMN, with the Dorsal Attention, Salience/Ventral Attention, Limbic, and Control networks in intermediate positions, consistent with a sensorimotor-to-transmodal cortical hierarchy.

Gradient alterations at the global and network levels

G1 range and variance differed among groups. The range was lower in NHE and HE than in HCs ($F = 11.939$, $P < 0.001$, $\eta_p^2 = 0.196$; both pairwise $P < 0.001$), without a difference between the patient groups. Variance was likewise lower in NHE and HE than in HCs ($F = 11.211$, $P < 0.001$, $\eta_p^2 = 0.186$; pairwise $P = 0.001$ and $P < 0.001$, respectively), again without a patient-group difference (Fig. 3A, B; Supplementary Table 1). Both patient groups showed compression at the two ends of G1 and a relative increase in its intermediate portion (Fig. 3C).

Network-level differences were observed mainly in the Somatomotor, Limbic, Control, and Default Mode networks (Fig. 4; Supplementary Table 1). Somatomotor G1 was higher in NHE and HE than in HCs ($F = 14.186$, $P < 0.001$, $\eta_p^2 = 0.225$; pairwise $P = 0.002$ and $P < 0.001$), with no difference between the patient groups. Limbic G1 was lower in HE than in HCs and NHE ($F = 6.522$, $P = 0.004$, $\eta_p^2 = 0.117$; pairwise $P = 0.013$ and 0.004). Control and Default Mode G1 were lower in both patient groups than in HCs (Control:

F = 8.284, P = 0.001, η_p^2 = 0.145; Default Mode: F = 8.305, P = 0.001, η_p^2 = 0.145; both pairwise P = 0.003), without NHE-HE differences. Hedges' g values are shown in Supplementary Fig. 1. No global or network-level G2 or G3 measure survived FDR correction.

Cortical spatial distribution of principal gradient (G1) alterations

The three groups retained a similar overall G1 topography (Fig. 5A). Within this shared organization, both patient groups had higher G1 values in bilateral somatomotor and posterior parietal cortices, extending into the left parietal operculum, than HCs. Lower values were located mainly in bilateral lateral and medial prefrontal cortex and parietal association cortex related to the DMN (Fig. 5B; Supplementary Table 2).

Spatial overlap analysis identified 40 parcels with concordant alterations in both patient groups: increased G1 values occurred mainly in bilateral somatomotor and posterior parietal cortices, whereas decreased values occurred in frontoparietal association cortex. NHE-specific changes were concentrated in lateral and medial prefrontal cortex, left parietal association cortex, and the right temporo-occipito-parietal junction. HE-specific changes were more widely distributed and additionally involved bilateral lateral temporal cortices and temporal poles, posterior parietal and frontal association cortex, and medial Salience/Ventral Attention regions (Fig. 6A; Supplementary Tables 2–4). The direct HE-NHE comparison identified one significant parcel in the right temporal pole of the Limbic network (RH_Limbic_TempPole_4; difference = − 1.649, t = − 4.060, FDR-adjusted P = 0.040; Fig. 6B; Supplementary Table 5).

Associations of principal gradient alterations with disease severity and cognitive function

In the pooled patient sample, higher blood ammonia was associated with higher Somatomotor G1 (r = 0.510, P < 0.001) and lower Control and Default Mode G1 (r = − 0.499 and − 0.488, respectively; both P < 0.001). Higher Child-Pugh scores were associated with lower Limbic and Default Mode G1 (r = − 0.282, P < 0.05; and r = − 0.364, P < 0.01), and higher MELD scores with lower Default Mode G1 (r = − 0.304, P < 0.05) (Fig. 7A).

Lower PHES scores were associated with higher Somatomotor G1 (r = − 0.326, P = 0.019) and lower Limbic, Control, and Default Mode G1 (r = 0.414, 0.336, and 0.419, respectively; P < 0.01, P < 0.05, and P = 0.002). Lower MoCA scores were associated with lower G1 in these three higher-order networks (r = 0.279, 0.355, and 0.410; all P < 0.05), and lower MMSE scores with lower Default Mode G1 (r = 0.354, P < 0.01). Representative partial correlation plots are shown in Fig. 7B-E.

Regional correlations were consistent with the network-level findings. Higher ammonia and greater liver disease severity were associated mainly with higher somatomotor values and lower values in DMN-

related prefrontal, parietal, and temporal association cortices and bilateral temporal poles. Better cognition showed the opposite pattern. Complete parcel-level results are provided in Supplementary Table 6.

Robustness analyses

The principal differences in global G1 range and variance, network-level G1 values, and parcel-level spatial patterns remained after additional adjustment for mean FD (Supplementary Tables 7–11). The main global and network findings were also consistent across 5%, 10%, and 15% connectivity sparsity thresholds (Supplementary Table 12).

Discussion

In this study, functional connectivity gradients were used to characterize cortical organization across the cirrhosis–HE spectrum. Compared with HCs, both NHE and HE showed reduced G1 range and variance, with preserved gradient mean and no significant changes in G2 or G3, indicating predominant abnormalities along the sensorimotor-to-transmodal axis. At the network level, both groups showed higher somatomotor G1 and lower control and default mode G1, whereas HE additionally showed lower limbic G1. At the parcel level, NHE and HE exhibited widespread and directionally consistent abnormalities relative to HCs, while the direct HE–NHE difference was localized to the right temporal pole. These alterations were associated with blood ammonia, liver disease severity, and cognitive performance. Overall, the findings indicate a predominantly shared disruption of the principal cortical hierarchy across NHE and HE, accompanied by more selective HE-associated alterations.

The cortical functional hierarchy is a fundamental principle of large-scale brain organization, supporting the progressive integration of information from primary sensorimotor processing to higher-order transmodal cognitive systems [11, 12]. In the present study, reduced G1 range and variance, together with preserved gradient mean and unchanged G2 and G3, suggest preferential compression of the principal hierarchical axis rather than a generalized shift across gradient space. Network-level findings further clarified this pattern: higher somatomotor G1 together with lower control and default mode G1 brought the two ends of the principal gradient closer together. Because gradient position reflects similarities in whole-brain connectivity profiles across cortical regions [12, 14], this convergence is consistent with reduced functional differentiation between primary sensorimotor and higher-order transmodal systems. Previous studies have reported abnormalities in somatomotor, cognitive control, and default mode networks in cirrhosis [6–9], while stage-related changes in sensorimotor- and visual-related connectivity have also been observed with HE progression [33]. Similar contraction of the principal functional hierarchy has been reported in other clinical conditions, including Cushing's disease and subthreshold depression [17, 18]. Previous gradient work in cirrhosis has likewise demonstrated stage-related disruption of macroscale cortical hierarchy [20]. Together, these findings suggest that reduced differentiation between primary and transmodal systems may represent a systems-level feature of cirrhosis-related brain dysfunction.

Within this broader hierarchical disturbance, HE-associated alterations were concentrated in the temporolimbic system. Limbic G1 was lower in HE than in both HCs and NHE, and the direct parcel-level HE–NHE comparison identified a significant difference in the right temporal pole. Although HE showed more spatially extensive abnormalities relative to HCs, the direct HE–NHE differences were regionally selective rather than broadly distributed. The limbic network mainly encompasses orbitofrontal and anterior temporal regions [30], while the temporal pole is a higher-order association area broadly connected with sensory, language, paralimbic, and default-semantic systems and contributes to semantic and socioemotional integration [34–37]. Previous work has similarly implicated right temporal pole dysfunction in the progression from cirrhosis to MHE and linked it to poorer PHES performance [10]. Thus, the temporolimbic findings may represent a more selective component of HE-associated cortical reorganization superimposed on the broader hierarchical abnormalities observed across cirrhosis.

Clinical correlations further supported the relevance of these gradient abnormalities. Across patients with cirrhosis, higher blood ammonia levels were associated with higher somatomotor G1 and lower control and default mode G1, whereas greater liver disease severity was mainly associated with lower limbic and default mode G1. Poorer PHES, MoCA, and MMSE performance showed broadly corresponding associations. At the parcel level, these relationships mainly involved the sensorimotor cortex, default mode–related association cortex, and temporal pole. The right temporal pole parcel that differed between HE and NHE was associated with PHES performance, while a neighboring temporal pole parcel was also related to blood ammonia, liver disease severity, and multiple cognitive measures. Previous studies have likewise linked functional network abnormalities in MHE to PHES performance and altered cerebral metabolism [38, 39]. Mechanistically, impaired hepatic detoxification and portosystemic shunting [40] may promote the accumulation of ammonia and other neurotoxic substances, which can interact with systemic inflammation to disrupt large-scale brain networks through astrocytic dysfunction, neuroinflammation, and neurotransmitter imbalance [1, 41–43]. Nevertheless, these cross-sectional associations do not establish causality, and pooled patient correlations may partly reflect between-group differences.

This study has several limitations. First, this was a single-center, cross-sectional study with relatively small numbers within individual HE subtypes. The HE group included patients with covert HE, overt HE, and a recent history of overt HE, limiting subtype-specific interpretation and preventing inference about longitudinal progression. Second, HE-related treatment may affect blood ammonia levels, cognitive performance, and resting-state brain function, and medication-related confounding could not be fully excluded. Moreover, because the HE and NHE groups differed in liver disease severity, additional alterations observed in HE cannot be attributed exclusively to HE itself. Third, systemic inflammation and portosystemic shunt burden were not systematically assessed. Fourth, field-map- or reversed-phase-encoding-based susceptibility distortion correction was unavailable; therefore, the right temporal pole finding should be interpreted cautiously given the susceptibility of anterior temporal regions to EPI-related signal loss and geometric distortion. Finally, the Schaefer atlas is restricted to the cerebral cortex and does not include subcortical or cerebellar regions. Larger multicenter longitudinal studies with

refined clinical stratification and multimodal imaging are needed to determine how these hierarchical abnormalities evolve across the course of cirrhosis and HE.

Conclusion

NHE and HE were characterized by a predominantly shared disruption of the sensorimotor-to-transmodal cortical hierarchy, indicating that large-scale hierarchical abnormalities are already evident in cirrhosis without HE and remain prominent in patients with HE. Additional HE-associated alterations were more selectively distributed, particularly within temporolimbic regions. These findings support altered cortical functional hierarchy as a clinically relevant systems-level phenotype across the cirrhosis–HE spectrum.

Abbreviations

DMN	default mode network
eGFR	estimated glomerular filtration rate
FC	functional connectivity
FD	framewise displacement
FDR	false discovery rate
G1	first functional connectivity gradient
G2	second functional connectivity gradient
G3	third functional connectivity gradient
HC	healthy control
HE	hepatic encephalopathy
MELD	Model for End-Stage Liver Disease
MHE	minimal hepatic encephalopathy
MMSE	Mini-Mental State Examination
MoCA	Montreal Cognitive Assessment
MRI	magnetic resonance imaging
NHE	cirrhosis without hepatic encephalopathy
PHES	Psychometric Hepatic Encephalopathy Score
rs-fMRI	resting-state functional magnetic resonance imaging

Declarations

Acknowledgments

The authors thank all participants for their participation in this study.

Author contributions

M.M., G.W., and X.W. contributed equally to this work. M.M., A.L.S., and L.F. conceived and designed the study. G.W., S.H., C.H., and L.C. contributed to data acquisition and methodology. M.M., G.W., and X.W. performed the analyses and visualization. H.H., A.L.S., and L.F. supervised the study and acquired funding. M.M. drafted the manuscript, and L.F. revised it. All authors read and approved the final manuscript.

Funding

This work was supported by the School Management Projects of Fujian University of Traditional Chinese Medicine (X2025004 and X2025012), the Joint Funds for Science and Technology Innovation of Fujian Province (2025Y9716), and the Natural Science Foundation of Fujian Province (2026J001840).

Data availability

The data are not publicly available due to privacy and ethical restrictions. Summary statistical data are available from the corresponding author upon reasonable request.

Ethics approval and consent to participate

The study was conducted in accordance with the Declaration of Helsinki and was approved by the institutional review board of the 900th Hospital of the Joint Logistics Support Force (approval no. 2025-087). Written informed consent was obtained from all participants.

Consent for publication

Not applicable.

Competing interests

The authors declare no competing interests.

References

1. Häussinger D, Dhiman RK, Felipo V, et al. Hepatic encephalopathy. Nat Rev Dis Primers. 2022;8:43. https://doi.org/10.1038/s41572-022-00366-6.
2. Chinese Society of Hepatology, Chinese Medical Association. Chinese guidelines on the management of hepatic encephalopathy in cirrhosis (2024). Chin J Hepatol. 2024;32:799–812. https://doi.org/10.3760/cma.j.cn501113-20240630-00309.

3. European Association for the Study of the Liver. EASL Clinical Practice Guidelines on the management of hepatic encephalopathy. J Hepatol. 2022;77:807–24. https://doi.org/10.1016/j.jhep.2022.06.001.
4. Kibble H, Shawcross DL. The assessment and management of cirrhotic patients with encephalopathy. United Eur Gastroenterol J. 2024;12:187–93. https://doi.org/10.1002/ueg2.12530.
5. Patidar KR, Thacker LR, Wade JB, et al. Covert hepatic encephalopathy is independently associated with poor survival and increased risk of hospitalization. Am J Gastroenterol. 2014;109:1757–63. https://doi.org/10.1038/ajg.2014.264.
6. Jiao Y, Wang XH, Chen R, et al. Predictive models of minimal hepatic encephalopathy for cirrhotic patients based on large-scale brain intrinsic connectivity networks. Sci Rep. 2017;7:11512. https://doi.org/10.1038/s41598-017-11196-y.
7. Qin B, Liang S, Tang S, et al. Altered spontaneous brain activity in cirrhotic patients with minimal hepatic encephalopathy: a meta-analysis of resting-state functional imaging. Brain Sci. 2023;13:960. https://doi.org/10.3390/brainsci13060960.
8. Chen HJ, Jiao Y, Zhu XQ, et al. Brain dysfunction primarily related to previous overt hepatic encephalopathy compared with minimal hepatic encephalopathy: resting-state functional MR imaging demonstration. Radiology. 2013;266:261–70. https://doi.org/10.1148/radiol.12120026.
9. Dong QY, et al. Metabolic disorder and functional disturbance in the central executive network in minimal hepatic encephalopathy. Cereb Cortex. 2024;34(2):bhae036. https://doi.org/10.1093/cercor/bhae036.
10. Cai LM, Shi JY, Dong QY, et al. Aberrant stability of brain functional architecture in cirrhotic patients with minimal hepatic encephalopathy. Brain Imaging Behav. 2022;16:2258–67. https://doi.org/10.1007/s11682-022-00696-9.
11. Mesulam MM. From sensation to cognition. Brain. 1998;121:1013–52. https://doi.org/10.1093/brain/121.6.1013.
12. Margulies DS, Ghosh SS, Goulas A, et al. Situating the default-mode network along a principal gradient of macroscale cortical organization. Proc Natl Acad Sci U S A. 2016;113:12574–79. https://doi.org/10.1073/pnas.1608282113.
13. Huntenburg JM, Bazin PL, Margulies DS. Large-scale gradients in human cortical organization. Trends Cogn Sci. 2018;22:21–31. https://doi.org/10.1016/j.tics.2017.11.002.
14. Vos de Wael R, Benkarim O, Paquola C, et al. BrainSpace: a toolbox for the analysis of macroscale gradients in neuroimaging and connectomics datasets. Commun Biol. 2020;3:103. https://doi.org/10.1038/s42003-020-0794-7.
15. Hong SJ, Vos de Wael R, Bethlehem RAI, et al. Atypical functional connectome hierarchy in autism. Nat Commun. 2019;10:1022. https://doi.org/10.1038/s41467-019-08944-1.
16. Dong D, Yao D, Wang Y, et al. Compressed sensorimotor-to-transmodal hierarchical organization in schizophrenia. Psychol Med. 2023;53:771–84. https://doi.org/10.1017/S0033291721002129.

17. Shang G, Zhou T, Yu X, et al. Chronic hypercortisolism disrupts the principal functional gradient in Cushing's disease: A multi-scale connectomics and transcriptomics study. Neuroimage Clin. 2024;43:103652. https://doi.org/10.1016/j.nicl.2024.103652.
18. Yin X, Yang J, Xiang Q, et al. Brain network hierarchy reorganization in subthreshold depression. Neuroimage Clin. 2024;42:103594. https://doi.org/10.1016/j.nicl.2024.103594.
19. Hu J, Chen G, Zeng Z, et al. Systematically altered connectome gradient in benign childhood epilepsy with centrotemporal spikes: Potential effect on cognitive function. Neuroimage Clin. 2024;43:103628. https://doi.org/10.1016/j.nicl.2024.103628.
20. Lin S, Qi R, Lin X, et al. Association between MRI-assessed patterns of connectome gradient and gene-expression profiles in two independent patient cohorts with hepatitis B virus-related cirrhosis. J Magn Reson Imaging. 2023;58:1863–74. https://doi.org/10.1002/jmri.28732.
21. Yoshiji H, Nagoshi S, Akahane T, et al. Evidence-based clinical practice guidelines for Liver Cirrhosis 2020. J Gastroenterol. 2021;56:593–619. https://doi.org/10.1007/s00535-021-01788-x.
22. Jophlin LL, Singal AK, Bataller R, et al. ACG clinical guideline: alcohol-associated liver disease. Am J Gastroenterol. 2024;119:30–54. https://doi.org/10.14309/ajg.0000000000002572.
23. Li SW, Wang K, Yu YQ, et al. Psychometric hepatic encephalopathy score for diagnosis of minimal hepatic encephalopathy in China. World J Gastroenterol. 2013;19:8745–51. https://doi.org/10.3748/wjg.v19.i46.8745.
24. Chinese Society of Gastroenterology, Chinese Medical Association. Chinese Consensus on Clinical Diagnosis and Management of Covert Hepatic Encephalopathy. J Dig Dis. 2025;26:268–85. https://doi.org/10.1111/1751-2980.70005.
25. Folstein MF, Folstein SE, McHugh PR. Mini-mental state: A practical method for grading the cognitive state of patients for the clinician. J Psychiatr Res. 1975;12:189–98. https://doi.org/10.1016/0022-3956(75)90026-6.
26. Nasreddine ZS, Phillips NA, Bedirian V, et al. The Montreal Cognitive Assessment, MoCA: A brief screening tool for mild cognitive impairment. J Am Geriatr Soc. 2005;53:695–9. https://doi.org/10.1111/j.1532-5415.2005.53221.x.
27. Pugh RN, Murray-Lyon IM, Dawson JL, et al. Transection of the oesophagus for bleeding oesophageal varices. Br J Surg. 1973;60:646–9. https://doi.org/10.1002/bjs.1800600817.
28. Kamath PS, Wiesner RH, Malinchoc M, et al. A model to predict survival in patients with end-stage liver disease. Hepatology. 2001;33:464–70. https://doi.org/10.1053/jhep.2001.22172.
29. Yan CG, Wang XD, Zuo XN, et al. DPABI: Data Processing & Analysis for (Resting-State). Brain Imaging Neuroinformatics. 2016;14:339–51. https://doi.org/10.1007/s12021-016-9299-4.
30. Yeo BTT, Krienen FM, Sepulcre J, et al. The organization of the human cerebral cortex estimated by intrinsic functional connectivity. J Neurophysiol. 2011;106:1125–65. https://doi.org/10.1152/jn.00338.2011.
31. Schaefer A, Kong R, Gordon EM, et al. Local-global parcellation of the human cerebral cortex from intrinsic functional connectivity MRI. Cereb Cortex. 2018;28:3095–114.

https://doi.org/10.1093/cercor/bhx179.
32. Coifman RR, Lafon S. Diffusion maps. Appl Comput Harmon Anal. 2006;21:5–30. https://doi.org/10.1016/j.acha.2006.04.006.
33. Sha G, Liu Y, Cao Y, et al. Structural and functional neural correlates of sensorimotor deficits in progression of hepatic encephalopathy. Magn Reson Lett. 2024;5(2):200156. https://doi.org/10.1016/j.mrl.2024.200156.
34. Buckner RL, Andrews-Hanna JR, Schacter DL. The brain's default network: anatomy, function, and relevance to disease. Ann N Y Acad Sci. 2008;1124:1–38. https://doi.org/10.1196/annals.1440.011.
35. Binder JR, Desai RH, Graves WW, et al. Where is the semantic system? A critical review and meta-analysis of 120 functional neuroimaging studies. Cereb Cortex. 2009;19:2767–96. https://doi.org/10.1093/cercor/bhp055.
36. Olson IR, Plotzker A, Ezzyat Y. The enigmatic temporal pole: a review of findings on social and emotional processing. Brain. 2007;130:1718–31. https://doi.org/10.1093/brain/awm052.
37. Pascual B, Masdeu JC, Hollenbeck M, et al. Large-scale brain networks of the human left temporal pole: a functional connectivity MRI study. Cereb Cortex. 2015;25:680–702. https://doi.org/10.1093/cercor/bht260.
38. Ju C, Yang L, Dai Z, et al. Dynamic network reconfiguration in hepatitis B cirrhosis secondary to mild hepatic encephalopathy: a multilayer network analysis. Quant Imaging Med Surg. 2026;16:163. https://doi.org/10.21037/qims-24-2442.
39. Huang HW, Liu RH, Zeng JY, et al. Alteration of dynamical degree centrality in brain functional network and its association with metabolic disorder in minimal hepatic encephalopathy. Neuroradiology. 2025;67:371–81. https://doi.org/10.1007/s00234-024-03470-4.
40. Praktiknjo M, Simon-Talero M, Romer J, et al. Total area of spontaneous portosystemic shunts independently predicts hepatic encephalopathy and mortality in liver cirrhosis. J Hepatol. 2020;72:1140–50. https://doi.org/10.1016/j.jhep.2019.12.021.
41. Shawcross DL, Davies NA, Williams R, et al. Systemic inflammatory response exacerbates the neuropsychological effects of induced hyperammonemia in cirrhosis. J Hepatol. 2004;40:247–54. https://doi.org/10.1016/j.jhep.2003.10.016.
42. Gallego-Durán R, Hadjihambi A, Ampuero J, et al. Ammonia-induced stress response in liver disease progression and hepatic encephalopathy. Nat Rev Gastroenterol Hepatol. 2024;21:774–91. https://doi.org/10.1038/s41575-024-00970-9.
43. Llansola M, Izquierdo-Altarejos P, Montoliu C, et al. Role of peripheral inflammation in minimal hepatic encephalopathy. Metab Brain Dis. 2024;39:1667–77. https://doi.org/10.1007/s11011-024-01417-5.

Figures

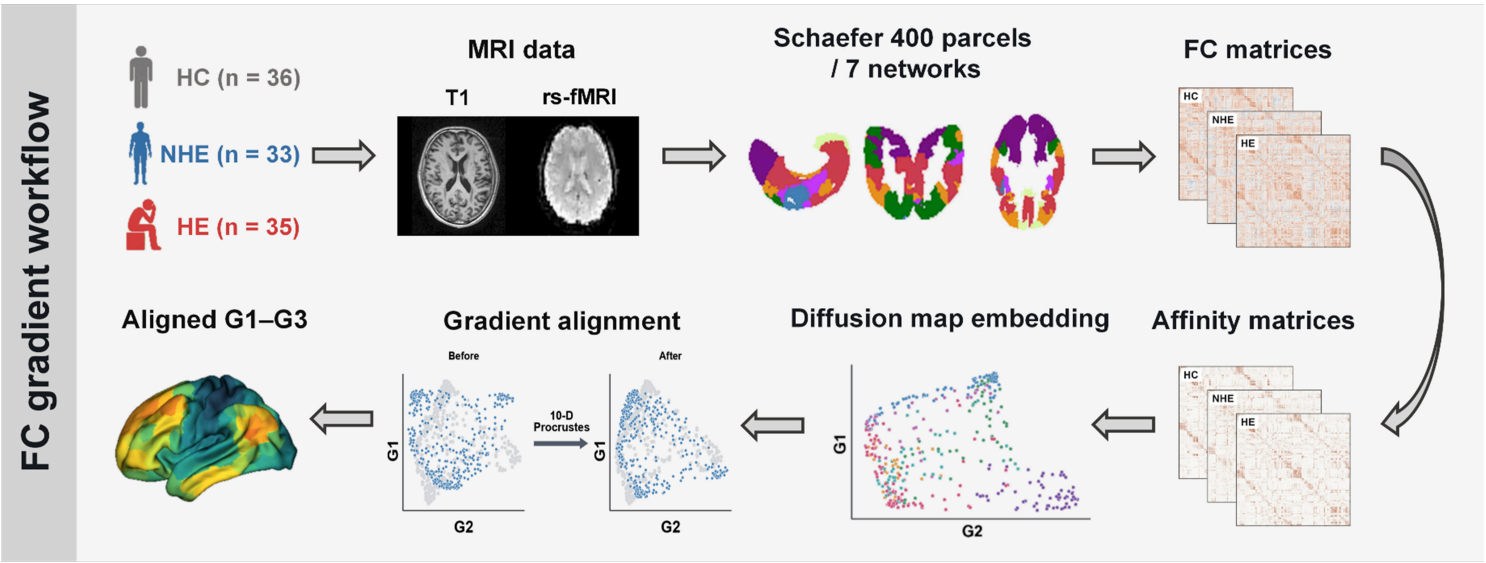


Figure 1

Functional connectivity gradient analysis workflow. Functional connectivity matrices based on the Schaefer-400 seven-network atlas were converted to affinity matrices, embedded using diffusion maps, and aligned by Procrustes rotation to obtain G1-G3. Abbreviations: HC, healthy control; NHE, cirrhosis without hepatic encephalopathy; HE, hepatic encephalopathy; FC, functional connectivity.

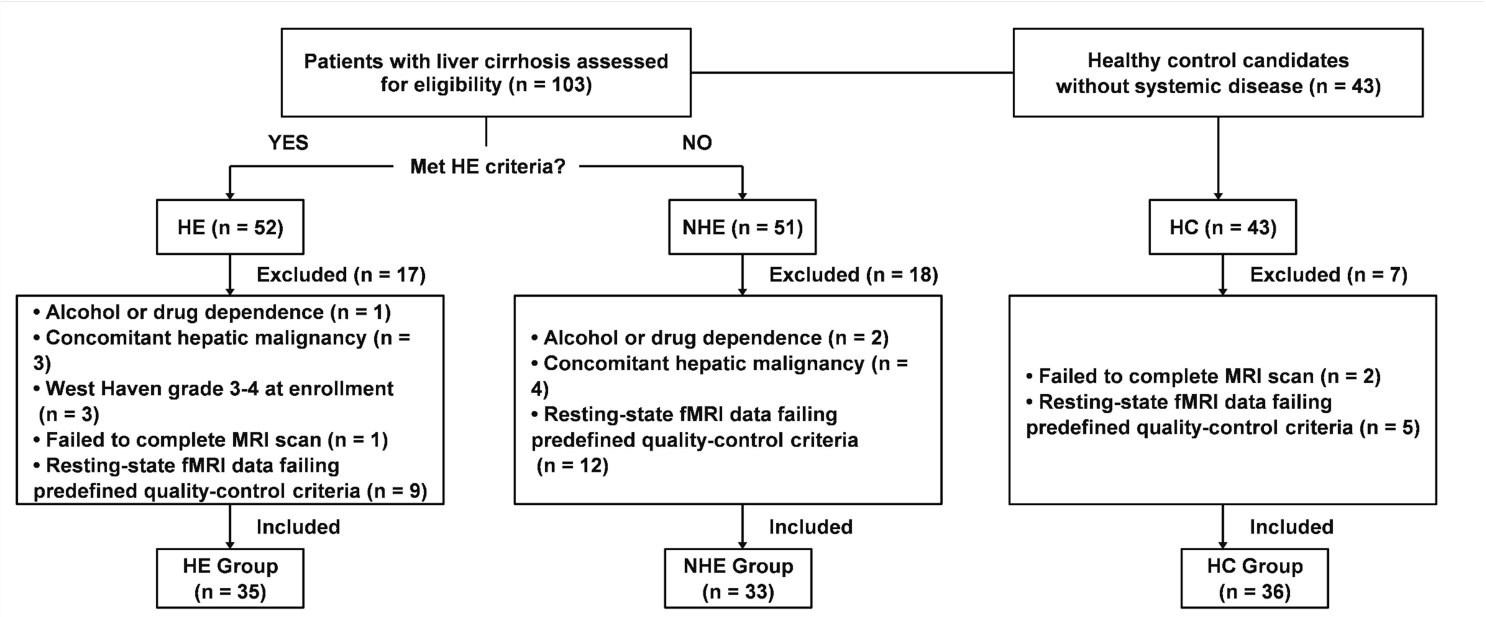


Figure 2

Participant screening, exclusion, and enrollment. Abbreviations: HC, healthy control; NHE, cirrhosis without hepatic encephalopathy; HE, hepatic encephalopathy.

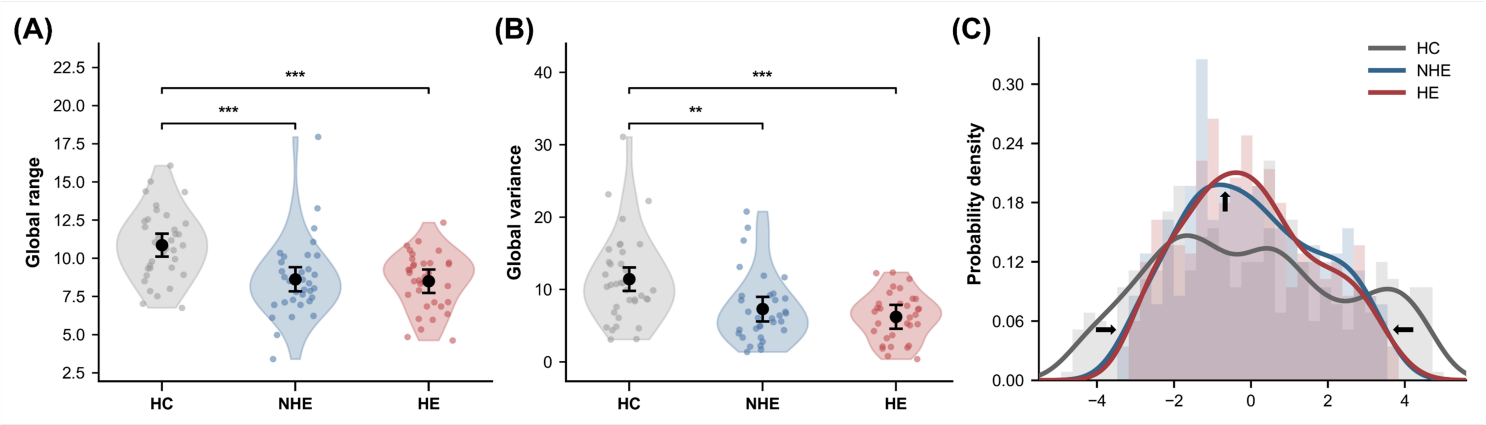


Figure 3

Global G1 characteristics. (A) Global range and (B) variance of G1 across groups. Violin plots show covariate-adjusted individual values; black dots and error bars indicate estimated marginal means and 95% confidence intervals. (C) Distribution of covariate-adjusted parcel-wise G1 scores; bars and lines indicate probability density and kernel density, respectively. Models were adjusted for age, sex, and education, with FDR-corrected pairwise comparisons. *P < 0.05, **P < 0.01, ***P < 0.001. Abbreviations: G1, first functional connectivity gradient; HC, healthy control; NHE, cirrhosis without hepatic encephalopathy; HE, hepatic encephalopathy.

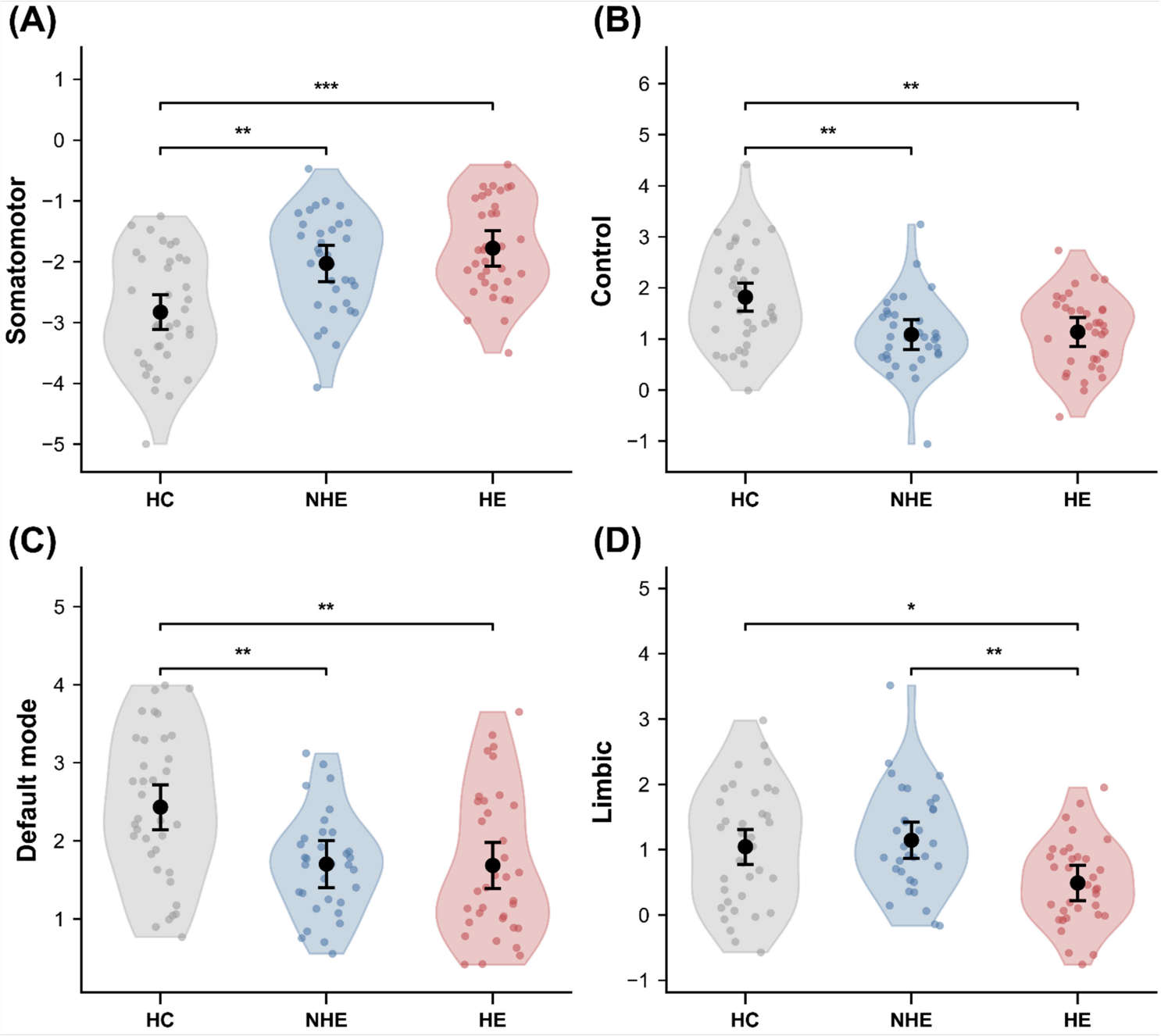


Figure 4

Network-level G1 differences. (A-D) Covariate-adjusted G1 scores in the Somatomotor, Control, Default Mode, and Limbic networks across groups. Violin plots show individual values; black dots and error bars indicate estimated marginal means and 95% confidence intervals. Models were adjusted for age, sex, and education, with FDR-corrected pairwise comparisons. *P < 0.05, **P < 0.01, ***P < 0.001. Abbreviations: G1, first functional connectivity gradient; HC, healthy control; NHE, cirrhosis without hepatic encephalopathy; HE, hepatic encephalopathy.

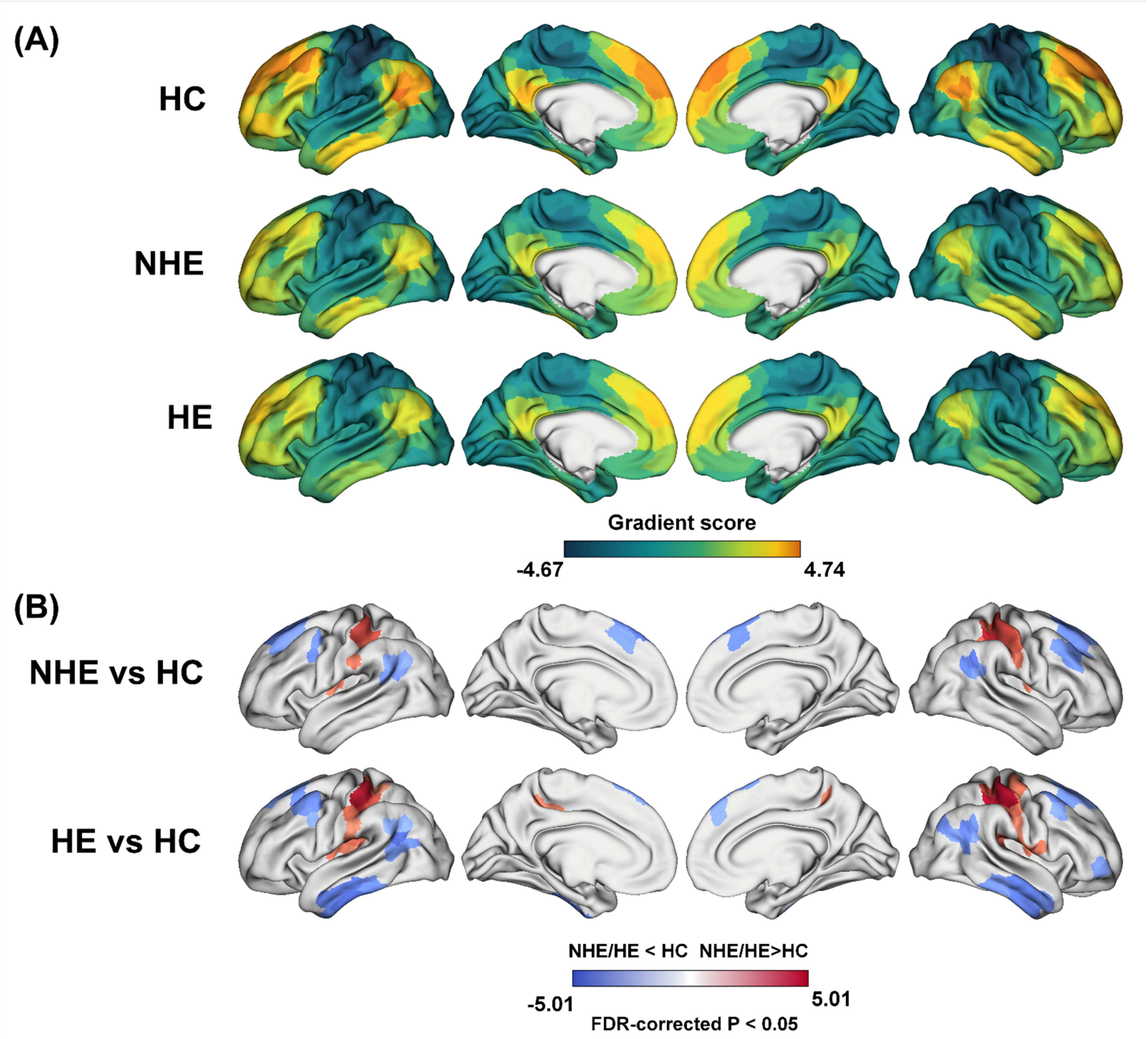


Figure 5

Cortical distribution of G1 and patient-control differences. (A) G1 topography in the HC, NHE, and HE groups. (B) FDR-corrected differences for NHE versus HC and HE versus HC ($P < 0.05$); blue and red indicate lower and higher G1 in patients, respectively. Models were adjusted for age, sex, and education. Abbreviations: G1, first functional connectivity gradient; HC, healthy control; NHE, cirrhosis without hepatic encephalopathy; HE, hepatic encephalopathy.

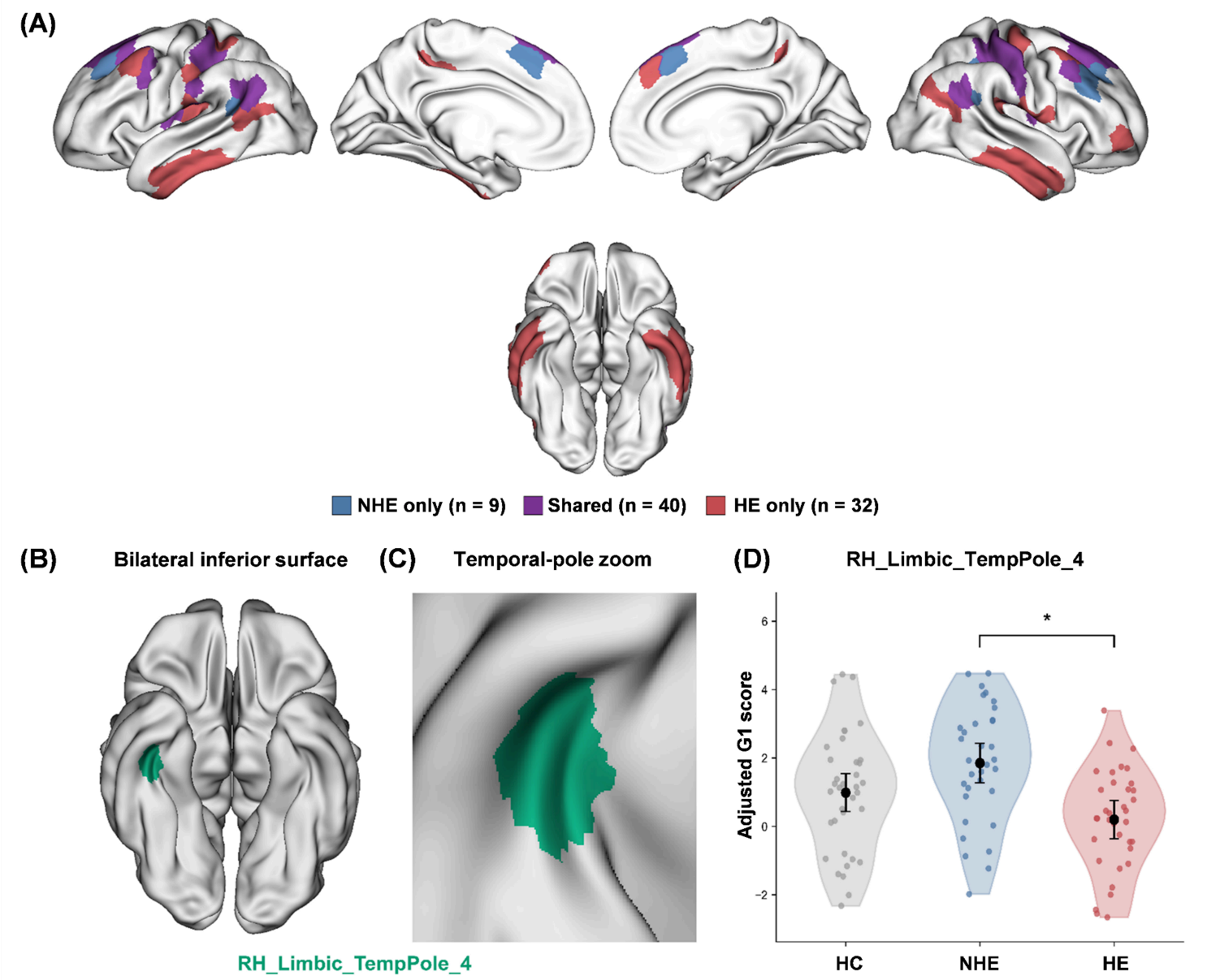


Figure 6

Shared and group-specific cortical G1 alterations. (A) Parcels altered only in NHE (blue), in both patient groups (purple), or only in HE (red), relative to HC. (B, C) Right temporal pole parcel (RH_Limbic_TempPole_4) showing the significant HE-NHE difference and its magnified location. (D) Covariate-adjusted G1 scores for this parcel; black dots and error bars indicate estimated marginal means and 95% confidence intervals. Models were adjusted for age, sex, and education, with FDR correction across parcels. *P < 0.05. Abbreviations: G1, first functional connectivity gradient; HC, healthy control; NHE, cirrhosis without hepatic encephalopathy; HE, hepatic encephalopathy.

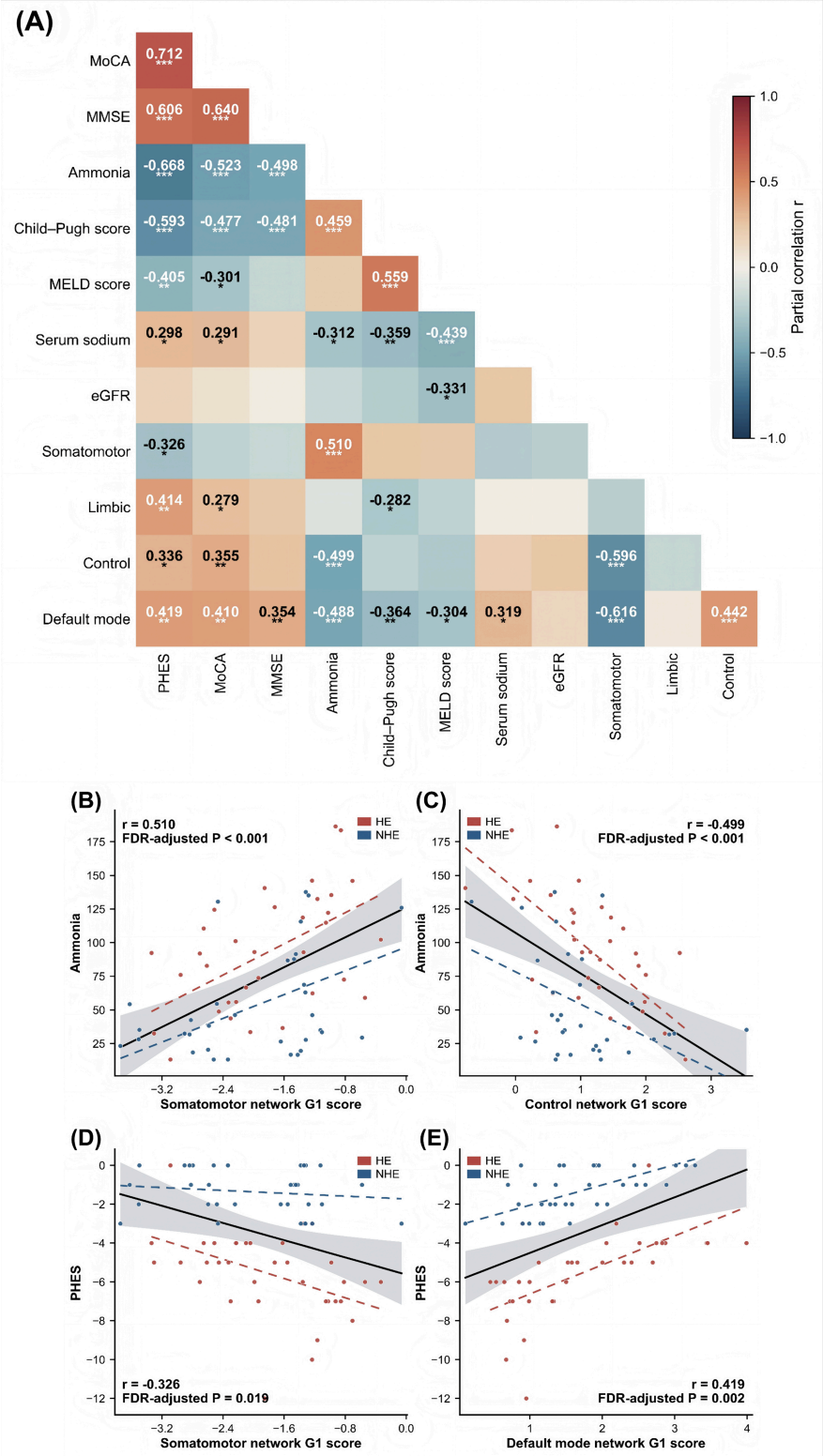


Figure 7

Associations of network-level G1 with clinical and cognitive measures. (A) Partial correlation matrix. (B) Positive correlation of blood ammonia with Somatomotor G1. (C) Negative correlation of blood ammonia with Control G1. (D) Negative correlation of PHES with Somatomotor G1. (E) Positive correlation of PHES with Default Mode G1. Analyses were adjusted for age, sex, and education and FDR-corrected. Solid lines and shaded areas indicate pooled regression fits and 95% confidence intervals; dashed lines indicate

group-specific fits. Abbreviations: G1, first functional connectivity gradient; HE, hepatic encephalopathy; NHE, cirrhosis without hepatic encephalopathy; PHES, Psychometric Hepatic Encephalopathy Score; MoCA, Montreal Cognitive Assessment; MMSE, Mini-Mental State Examination; MELD, Model for End-Stage Liver Disease; eGFR, estimated glomerular filtration rate.

Supplementary Files

This is a list of supplementary files associated with this preprint. Click to download.

- Supplementarymaterials.docx